

# **SAR Simulation Report for a MagSafe Battery Pack**

**Model: A2384**  
**FCC ID: BCGA2384**

**Date of Simulation:**

01/15/2021-04/20/2021

**Location:**

Apple Inc., Cupertino, CA, USA

---

## Table of Contents

<b>1</b>	<b>Introduction .....</b>	<b>3</b>
<b>2</b>	<b>Wireless Power Transfer System .....</b>	<b>5</b>
<b>3</b>	<b>Model Validation Methodology for Computational Exposure Assessment .....</b>	<b>5</b>
<b>4</b>	<b>Simulation Model Validation.....</b>	<b>6</b>
<b>4.1</b>	<b>H-field Measurements.....</b>	<b>6</b>
<b>4.2</b>	<b>H-field Simulations.....</b>	<b>7</b>
<b>4.3</b>	<b>Charger in stand-alone with Phone as Rx.....</b>	<b>8</b>
<b>4.4</b>	<b>Charger connected to power adapter with Phone as Rx .....</b>	<b>10</b>
<b>4.5</b>	<b>Charger (Tx) model Validation: .....</b>	<b>14</b>
<b>5</b>	<b>SAR Simulations .....</b>	<b>15</b>
<b>6</b>	<b>SAR Simulation Results .....</b>	<b>19</b>
<b>6.1</b>	<b>Charger in stand-alone with Phone as Rx.....</b>	<b>19</b>
<b>6.2</b>	<b>Charger connected to power adapter with Phone as Rx .....</b>	<b>21</b>
<b>6.3</b>	<b>Additional Exposure Cases: .....</b>	<b>23</b>
<b>7</b>	<b>Summary .....</b>	<b>26</b>
<b>8</b>	<b>Annex A: Specific Information for SAR Computational Modelling .....</b>	<b>27</b>

# 1 Introduction

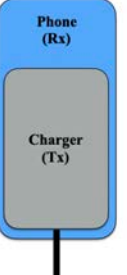
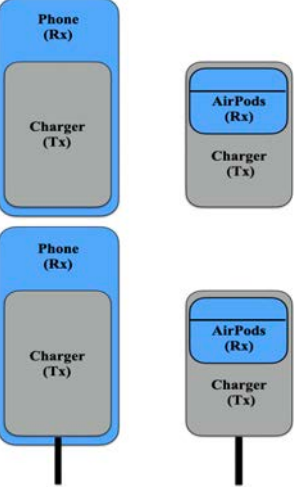
This report demonstrates RF exposure compliance using SAR simulations for WPT (Wireless Power Transfer) device, MagSafe Battery Pack (also called as “Charger” in this report) is designed to charge Apple Phones through closely coupled inductive field at 360 kHz. This WPT device can wirelessly charge external accessories in two modes: i) using Internal Battery (stand-alone) and ii) when connected to power adapter. This product has an internal battery and one WPT transmitter with magnets to secure the Charger to the client (Phone). Due to the Charger being held in place by magnets, it is expected that customers may use the charging function in portable use conditions; charging the Phone while making a call, or texting. Additional products will support true portable use, with the host-client pair able to be placed in a pocket or backpack.

All the possible use cases for this MagSafe Battery Pack and the certification methods are listed in Table 1. As shown in the Table 1, the Charger has two operating modes: (i) Charger in stand-alone mode and (ii) Charger connected to AC power adapter.

When the Charger is stand-alone mode and wirelessly charging a Phone (Rx), maximum power of 5 W can be delivered, whereas maximum power of 15W can be delivered to the Phone when the Charger is connected to power adapter.

Among all of the use cases listed in Table 1, only the legacy Phones and legacy AirPods will be evaluated using measurements and the rest of the use cases will be evaluated using SAR simulations for RF exposure compliance.

Table 1. Summary of normal use cases for the MagSafe Battery Pack and certification method for each use case.

Use Cases	Device	Frequency (kHz)	Max Power for nominal case	Certification Method
	New Phone	360	5W	SAR Simulations
	New Phone with Charger connected to power adapter	360	15W	SAR Simulations
	<p>Legacy Phone, Legacy AirPods Charger in stand-alone mode &amp;</p> <p>Legacy Phone, Legacy AirPods with Charger connected to power adapter.</p>	127.7	<p>5W (Phone)</p> <p>&amp;</p> <p>1W (AirPods)</p>	MPE measurements

We have found that the near-field H field strength may exceed the 1.63 A/m limit defined in §1.1310. Therefore, as permitted by §2.1093(d)(3) and Paragraph 3.d) of KDB 680106 D01, we use SAR numerical modeling to demonstrate compliance to the 1.6 W/kg localized 1-g SAR limit, due to the unavailability of SAR measurement tools and procedures.

Applying the SAR limit is also justified because:

1. The §1.1310 limits are intended for mobile whole-body exposure condition and are therefore far too stringent for local exposure conditions. In contrast, the §2.1093 local exposure limit is 20 times the whole-body SAR limit, and extremity exposure (held-in-hand) limit is 50 times higher.
2. The current H-field limits specified in international standards (IEEE and ICNIRP) are much higher than 1.63 A/m at 360 kHz.

The following sections describe the modeling, measured H-field, simulated H-field, simulated SAR, and simulated internal E-field for the use cases.

## **2 Wireless Power Transfer System**

The Charger consists of a transmitting coil with 11 turns and measures 7.5 uH nominally in free air. The Charger can be used either in stand-alone mode or by connecting it to external power adapter. The Phone coil consists of 13 turns and measures 9.06 uH nominally in free air. Both the coils are wound spirally and made of stranded wire.

When the Charger is connected to external power adapter and is used to wirelessly charge the Phone, maximum power of 15 W can be delivered to the Phone and only 5W when the Charger is using internal battery (or in stand-alone mode).

## **3 Model Validation Methodology for Computational Exposure Assessment**

The following steps are taken to show the validity of the model used for computational exposure simulations:

- 1) EM Simulation:
  - a. Import a CAD model that represents the actual product in the simulation tool.
  - b. Define material properties inside the product based on vendor's inputs.
  - c. Extract two-port network impedance matrix ([Z]) from the simulation.
- 2) Circuit Simulation:
  - a. Include the impedance matrix in the wireless power transfer circuit model.
  - b. Run circuit simulation and extract coils' current waveforms.
- 3) Field, H-field, and SAR Calculations:
  - a. Use the current waveforms to drive the EM simulation model.
  - b. Calculate H-field from simulation.

- c. Compare simulated H-field with measured H-field.
- d. Once a correlation is established, this model will be used for SAR simulations.

The entire workflow is summarized and shown in Fig. 1.

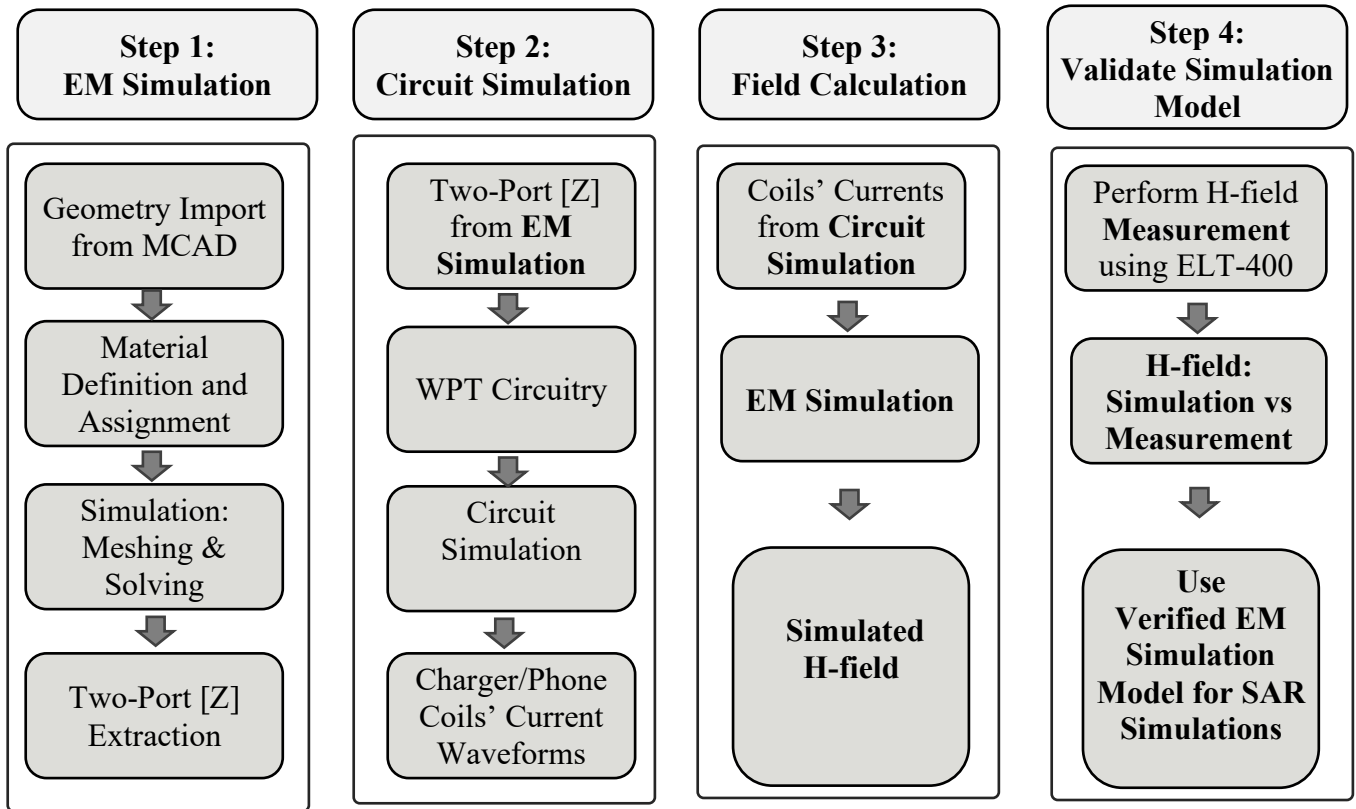


Figure 1: Model validation workflow for computational exposure assessment.

## 4 Simulation Model Validation

As an initial step, the simulation model is validated with H-field measurements for different use cases. Below sections provide the results of correlation study between the simulation model and the measurements (H-field) for different use-cases.

### 4.1 H-field Measurements

A Narda ELT-400 is used to measure the H-field above and below the DUT. A picture of the probe, an x-ray image of the probe, and the measurement setup are shown, below. The probe has three orthogonal loops with radius of 10mm. These loops are used to measure H-field in different directions. The distance from the DUT to the probe is 0mm. However, the loops are covered with a plastic shell of 6mm thickness. Therefore, the distance from the center of the probe to the DUT is 16mm. These factors have been considered in simulation when calculating the H-field.

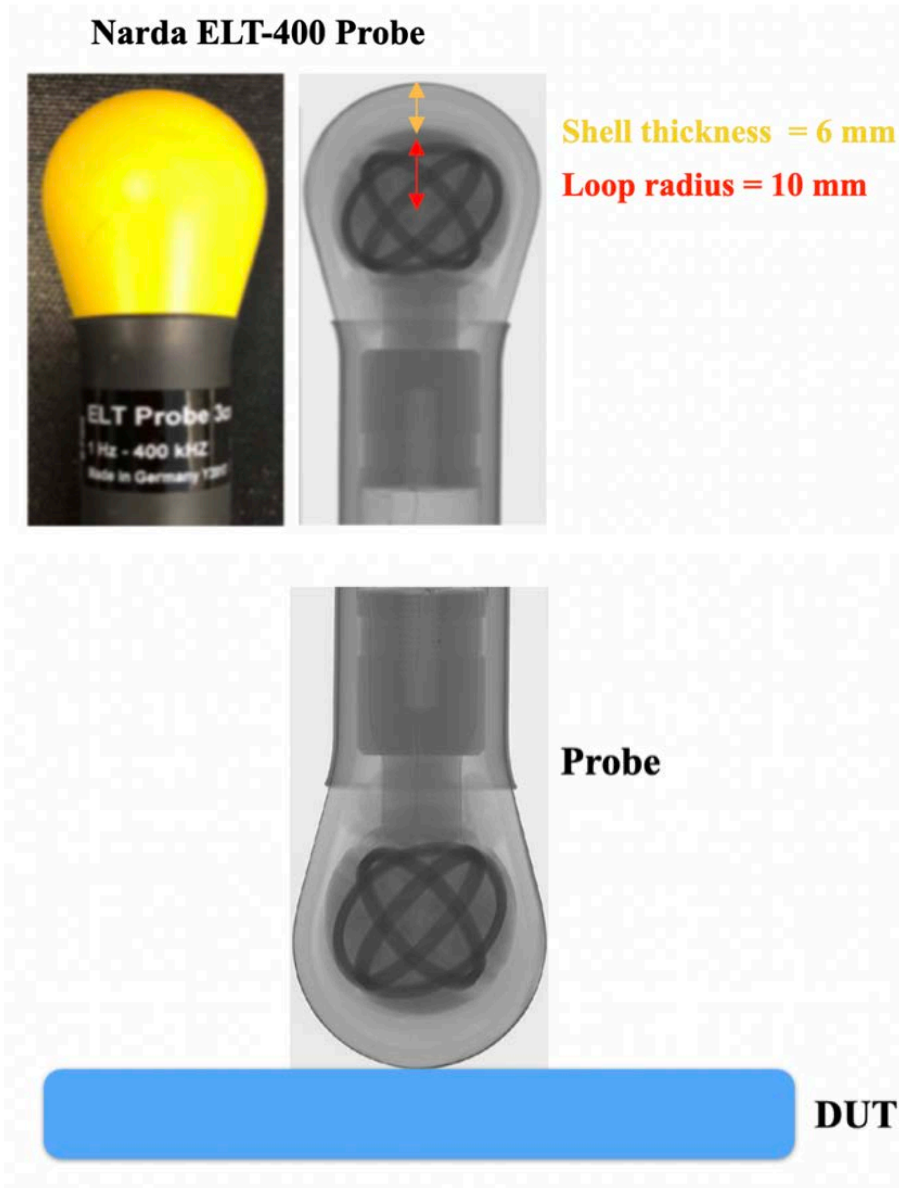


Figure 2: ELT-400 probe.

## 4.2 H-field Simulations

The Electromagnetics simulations are conducted using commercially available software ANSYS HFSS. In order to validate the simulation model, H-field measurements are made on the DUT (as explained above) and compared to the simulated model results. The validated model is then used for SAR simulations.

For the simulations, following Step 1 described above, the CAD file that represents the DUT is first imported. Then, the proper material properties are assigned at the operating frequency. After the simulation is completed, the two-port network [Z] was extracted and used with the WPT circuit model. This WPT model includes the charger source as well as the charging client-side

rectifier circuit. Solving the circuit using ANSYS Circuit tool, the proper excitation per transmitter (Charger) and receiver (Phone) coils are calculated. Later, these current waveforms are fed into the ANSYS HFSS to excite the coils and create H-field.

Correlation study between the simulation model and H-field measurements is done for the below scenarios.

- i. Charger in stand-alone with Phone as Rx (Max power delivered: 5 W)
- ii. Charger connected to power adapter with Phone as Rx (Max power delivered: 15 W)

### 4.3 Charger in stand-alone with Phone as Rx

When the Charger is used in stand-alone mode to wirelessly charge the Phone, under optimal placement, transmitter can deliver up to 5 W to the Phone receiver. However, if the Charger and Phone are misaligned/separated largely, the coupling efficiency will drop and consequently the maximum power that can be delivered will drop. To make our study comprehensive, we included the misalignment and displacement. As shown in Figs. 3 and 4, the Phone and the Charger can be unintentionally forced by user to be laterally misaligned or vertically separated. The misalignment and/or separation can change H-field's intensity and spatial distribution. Hence, several different misalignment and separation cases were selected and investigated to determine the worst-case scenario (i.e., highest H-field).

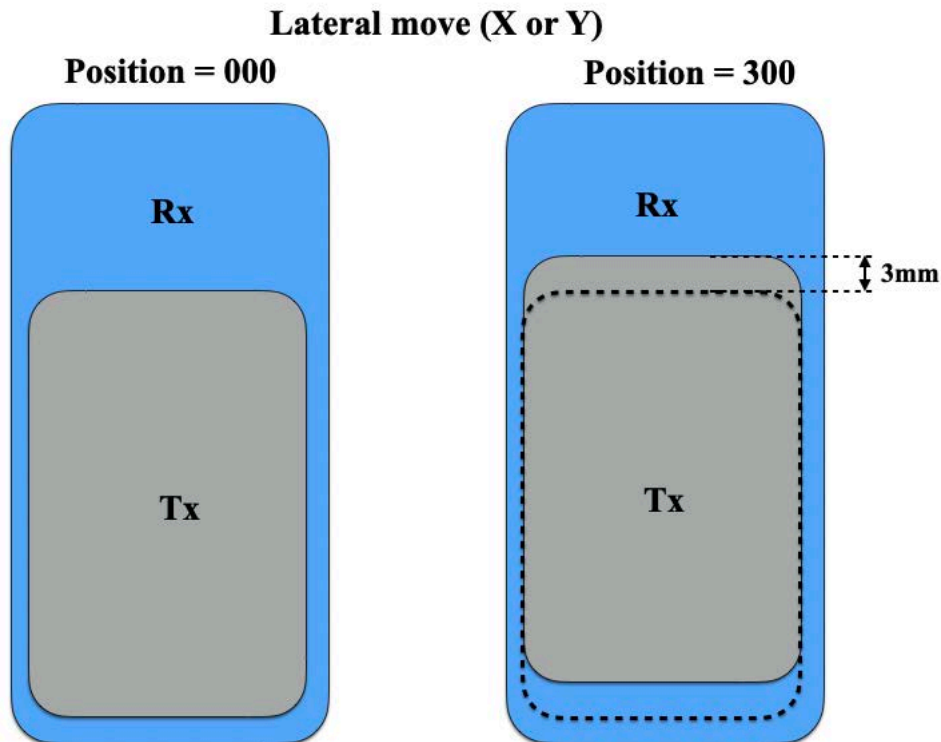


Figure 3: Lateral misalignment of Charger (Tx) and Phone (Rx).

**Vertical (z) move**



Figure 4: Vertical misalignment of Charger (Tx) and Phone (Rx).

Measurement setup for the H-field using Narda ELT-400 is shown below. For each side, the H-field probe is in contact with the EUT, scanning an area of 152 by 152 mm<sup>2</sup> with a step size of 2 mm. The maximum RMS H-field (A/m) is reported in the tables.

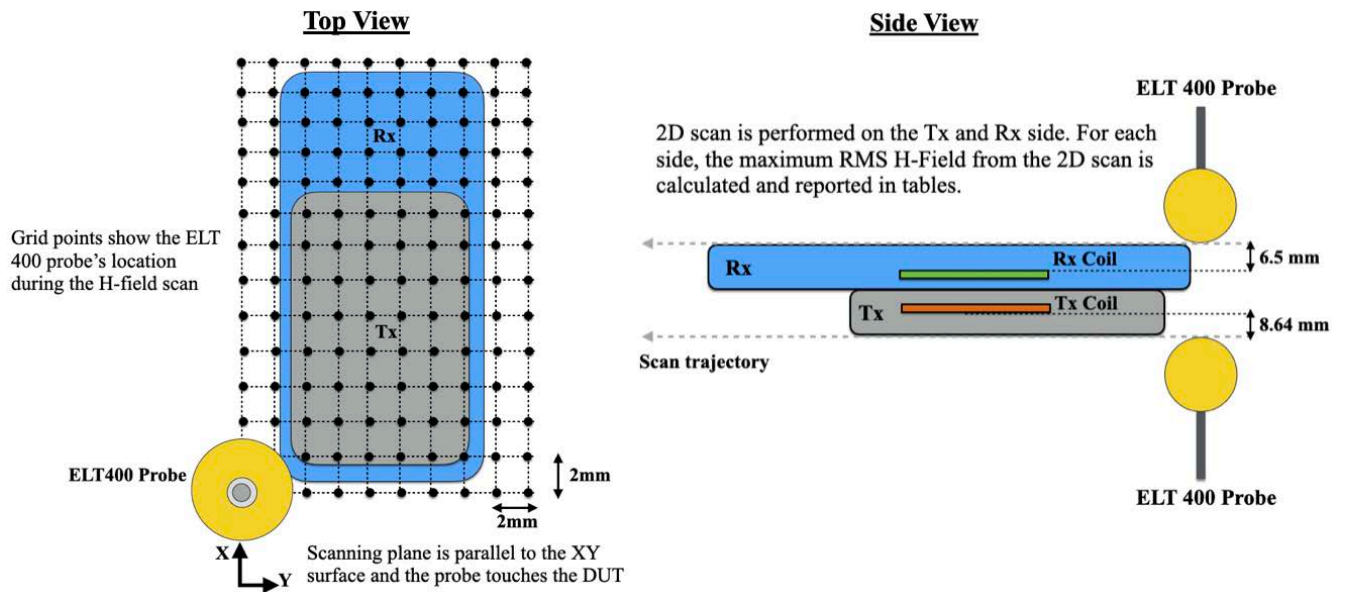


Figure 5: Scanning DUT to measure/calculate H field spatially.

H-field simulation and measurement results are compared for the Phone and Charger side when the Charger is in stand-alone and shown in below tables 2 and 3.

Table 2. Comparison of the simulated and measured H-field on the Phone side (Charger in stand-alone).

**Phone side RMS H-field (A/m)**

<b>Relative movement (X, Y, Z) from perfect alignment (mm)</b>	<b>Power delivered to Rx (W)</b>	<b>Measured H-field (A/m)</b>	<b>Simulated RMS H-field (A/m)</b>
(0, 0, 0)	5	0.5	0.33
(2, 0, 2)	5	0.58	0.59
(3, 0, 3)	3.5	0.59	0.76

Table 3. Comparison of the simulated and measured H-field on the Charger Side (Charger in stand-alone).

**Charger Side RMS H-field (A/m)**

<b>Relative movement (X, Y, Z) from perfect alignment (mm)</b>	<b>Power delivered to Rx (W)</b>	<b>Measured H-field (A/m)</b>	<b>Simulated RMS H-field (A/m)</b>
(0, 0, 0)	5	0.3	0.21
(2, 0, 2)	5	1.1	1.31
(3, 0, 3)	3.5	1.6	2.1

There is a good correlation between the simulation and measurement results. Also, as tables show, for aligned cases (i.e., zero lateral move), the Phone side shows relatively more radiation. This is mainly because the metallic housing of the Charger preforms as a good shield. While when there is a lateral misalignment, fields can leak from the sides and the H-field on the Charger side becomes more noticeable.

#### **4.4 Charger connected to power adapter with Phone as Rx**

Similarly, different misalignment and separation cases were investigated when the Charger is connected to power adapter to determine the worst-case scenario (i.e., highest H-field) as shown below.

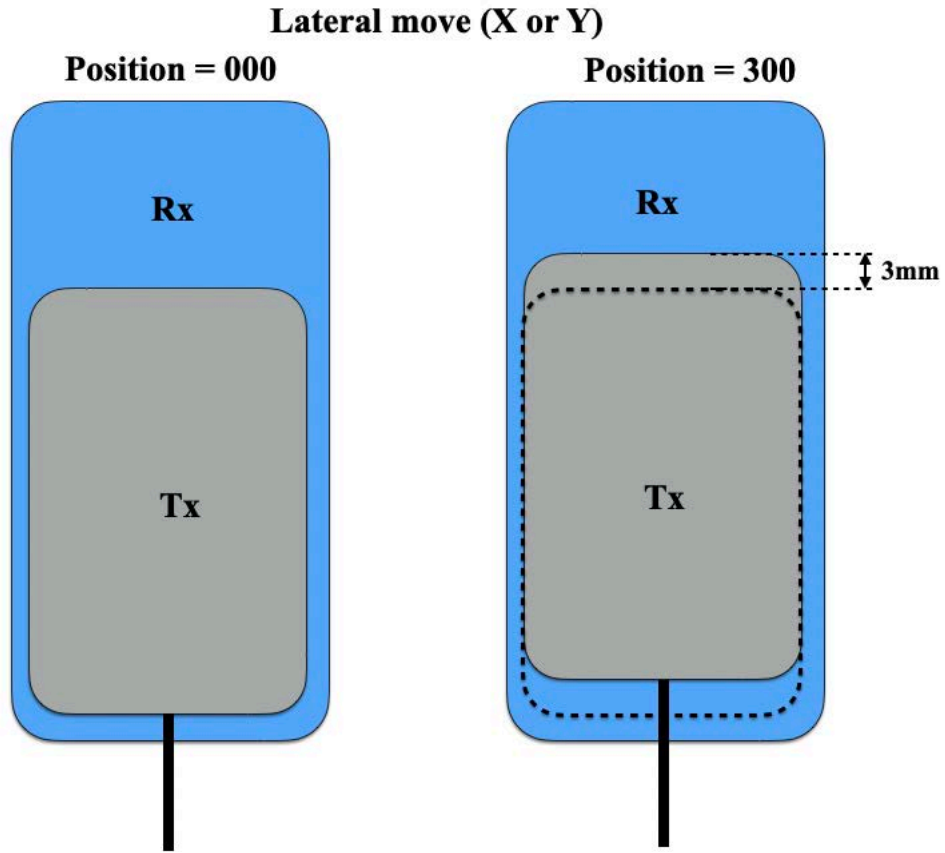


Figure 6: Lateral misalignment of Charger (Tx) and Phone (Rx).

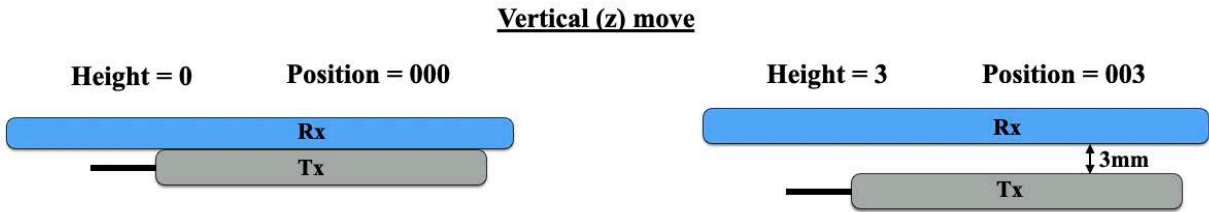


Figure 7: Vertical misalignment of Charger (Tx) and Phone (Rx).

Measurement setup for the H-field using Narda ELT-400 is shown below.

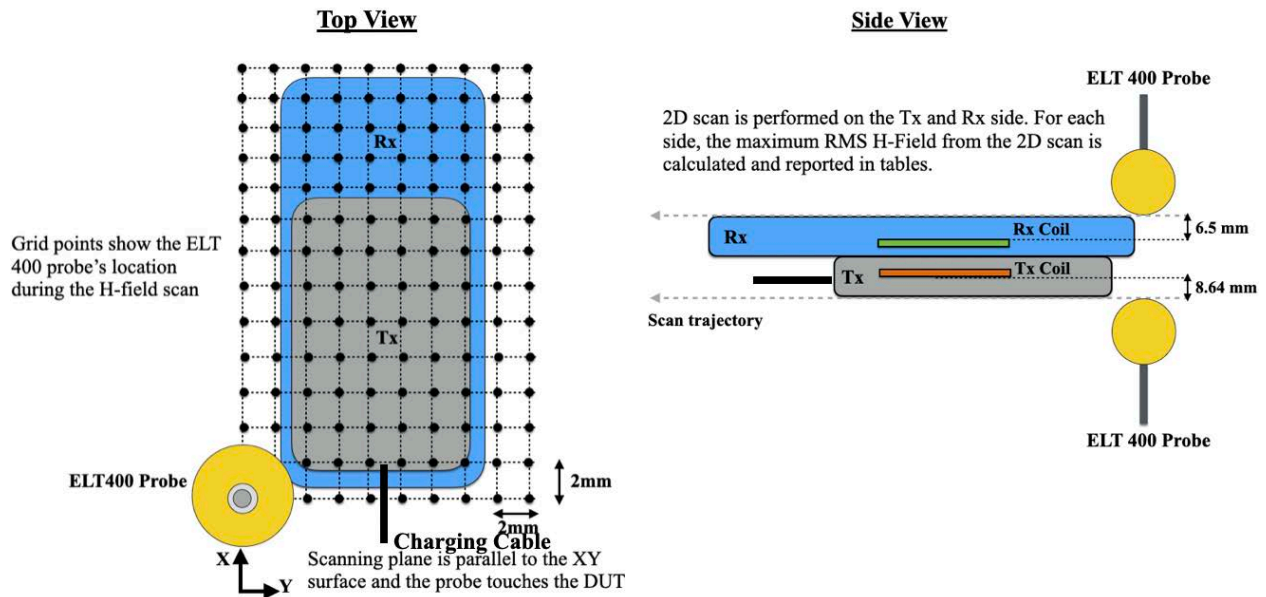


Figure 8: Scanning DUT to measure/calculate H field spatially.

H-field simulation and measurement results are compared for the Phone and Charger side when the Charger is connected to power adapter and shown in below tables 4 and 5.

Table 4. Comparison of the simulated and measured H-field on the Phone side (Charger connected to power adapter).

**Phone side RMS H-field (A/m)**

Relative movement (X, Y, Z) from perfect alignment (mm)	Power delivered to Rx (W)	Measured H-field (A/m)	Simulated RMS H-field (A/m)
(0, 0, 0)	15	0.42	0.41
(2, 0, 2)	15	0.58	0.78
(3, 0, 3)	7.5	0.6	0.81

Table 5. Comparison of the simulated and measured H-field on the Charger side(Charger connected to power adapter).

**Charger Side RMS H-field (A/m)**

<b>Relative movement (X, Y, Z) from perfect alignment (mm)</b>	<b>Power delivered to Rx (W)</b>	<b>Measured H-field (A/m)</b>	<b>Simulated RMS H-field (A/m)</b>
(0, 0, 0)	15	0.29	0.26
(2, 0, 2)	15	1.22	1.8
(3, 0, 3)	7.5	1.94	2.4

#### 4.5 Charger (Tx) model Validation:

To further evaluate the simulation model, we simulated and measured the Charger only scenario using the measurement setup shown in the inset of Fig. 12. Simulation model and measurements correlation is performed at a vertical distance away from the EUT and the probe is moved vertically in Z direction from 0 mm (probe center) to 150 mm until we reach the noise floor of the measurement probe.

Below Fig. 12 shows good correlation between the measurements and simulations, verifying the accuracy of the model. At distance very close to the EUT, simulations are little more conservative than measurements.

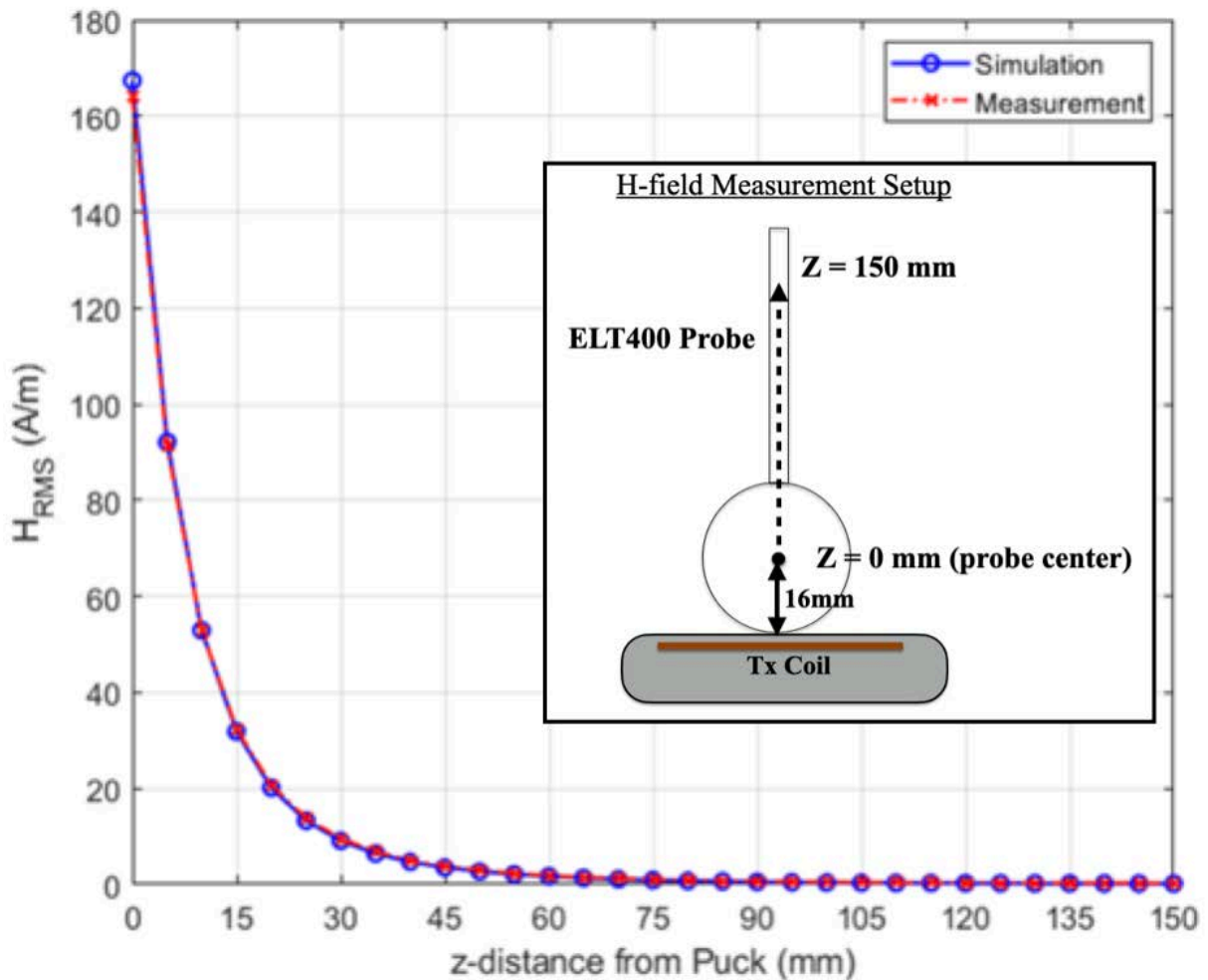


Figure 9: Correlating H-field variation from simulation and measurement when the probe moves from touching the Charger ( $z=0$ ) to 150 mm away.

## 5 SAR Simulations

With the correlation demonstrated between measurements and simulations, the same model is then used for SAR simulations with a phantom added in contact with the DUT. The simulations are computed on a 96 core CPU server with an available RAM of 4 Terabytes. For this simulation, the model run takes approximately 9 hours to complete.

The following steps are used for accurate SAR calculations:

- 1) Elliptical phantom used in body exposure measurements is commercially available from SPEAG: Outer dimensions of 600mm x 400mm x 150mm.
- 2) Homogeneous tissue material is used as liquid for desired frequency.
- 3) Power loss in phantom is calculated.
- 4) Divide power loss by mass density to calculate SAR.

$$SAR = \frac{P_l}{\rho}$$

$P_l$  = Power loss density

$\rho$  = Mass density

- 5) SAR is averaged over 1g tissue.
- 6) For SAR simulations, mass density of 1000 Kg/m<sup>3</sup> is used for the Phantom.

Here, a mass density of 1000 Kg/m<sup>3</sup> is used for the modeling and the simulation of the phantom.

### Human Tissue Material Properties:

The worst-case scenario has been identified to be when a user is holding the device in hand and taking a call or holding the phone on their body while charging. The electrical properties for body and hand layers are shown below. Since the SAR phantom is homogenous, using the layers' properties, the worst-case scenario is selected and applied for the phantom properties. Therefore, for the SAR simulations, the phantom that has conductivity of 0.5 and permittivity of 5016 are used.

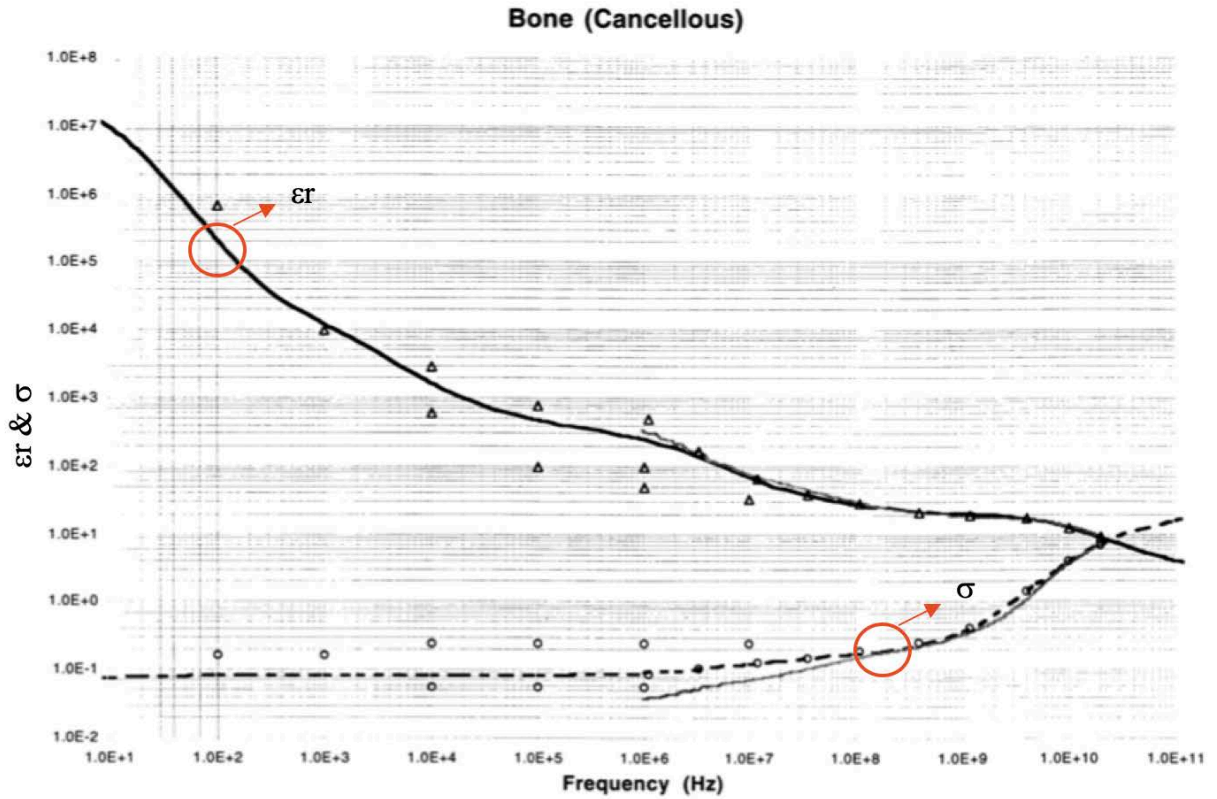
#### Electrical Properties:

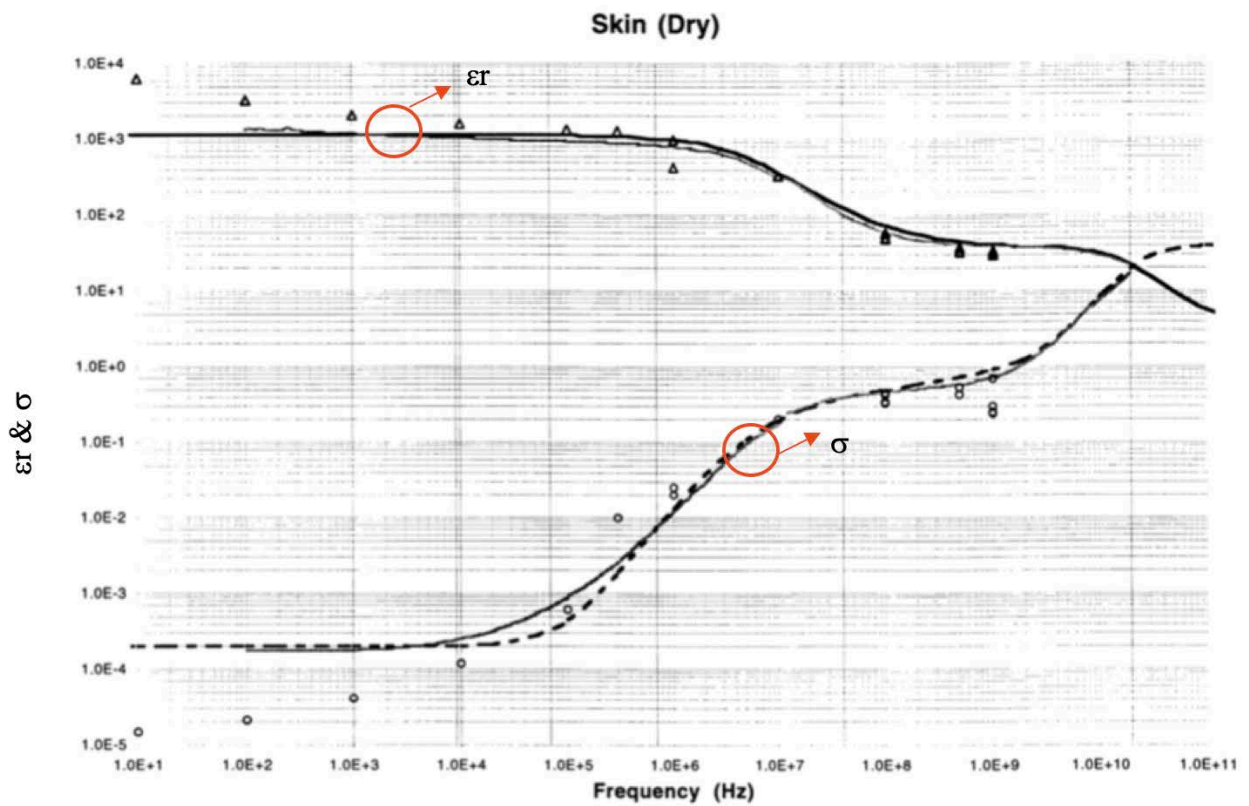
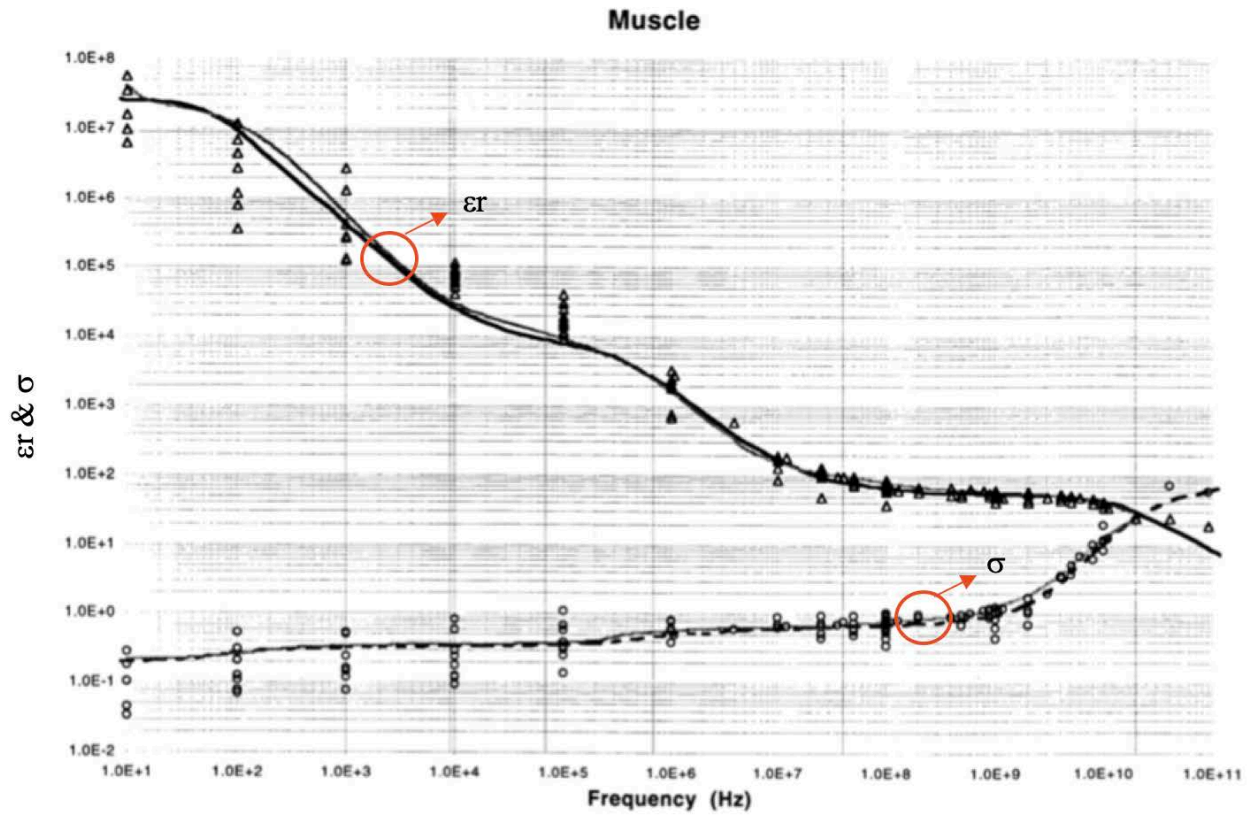
Based on our research this is what we recommend for er and sigma values for body layers.

Tissue	Thickness (mm)	Permittivity	Conductivity (S/m)
Skin	3	5016	0.16
Muscle	9	4666	0.5
Bone	20	1414	0.165
Worst case	100	5016	0.5

Based on our research this is what we recommend for er and sigma values for hand layers.

Tissue	Thickness (mm)	Permittivity	Conductivity (S/m)
Skin	2	5016	0.16
Muscle	2	4666	0.5
Bone	15	1414	0.165
Worst case	100	5016	0.5





## Mesh Adaptation

HFSS adapts the mesh based on the field strength. It is important to ensure the mesh is refined to capture SAR and E-field accurately. This can be done by using adaptive meshing technique available in HFSS.

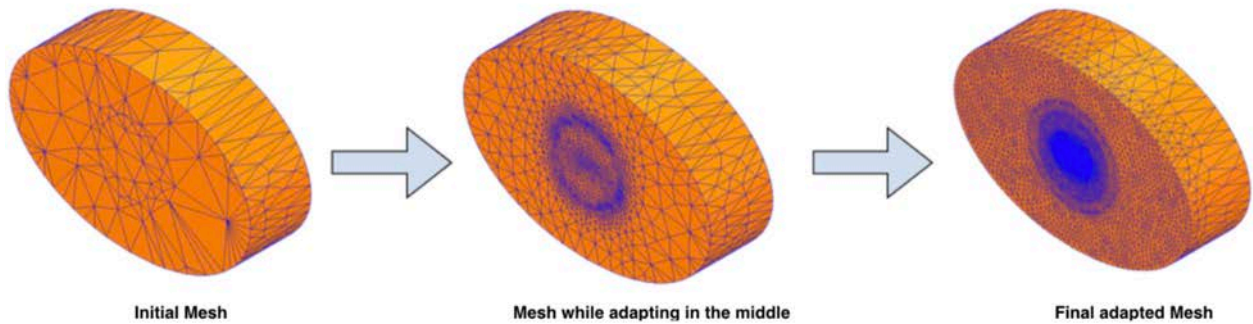


Figure 10: Initial mesh generation and then refinement through adaptive meshing technique in HFSS.

## 6 SAR Simulation Results

For all the exposure cases, dielectric properties (permittivity and conductivity) used for the phantom are fixed as permittivity: 5016, conductivity: 0.5 for SAR computation. The coil properties are also fixed, the Charger (transmitter) with 11 turns and measures 7.5 uH nominally in free air. The Phone (receiver) coil consists of 13 turns and measures 9.06 uH nominally in free air. Both the coils are wound spirally and made of stranded wire.

The following outputs are calculated and reported in the Table:

- a. Peak spatial 1-g average SAR in tissue.
- b. Peak spatially averaged electric field in tissue. Electric field is spatially averaged in a contiguous tissue volume of 2 mm x 2 mm x 2 mm.

We report the SAR results for the below cases:

- i. Charger in Stand-alone with Phone as Rx
- ii. Charger connected to AC power with Phone as Rx

### 6.1 Charger in stand-alone with Phone as Rx

Considering that the phantom can be in contact with the Phone or the back side of the Charger, there is a total of four scenarios.

**Exposure Case 000 (a):** Nominal configuration with perfect alignment and phantom placed above the Phone, hence exposed to Phone leakage.

**Exposure Case 000(b):** Nominal configuration with perfect alignment and phantom placed below the Charger, hence exposed to Charger leakage.

**Exposure Case 303 (a):** Misaligned configuration with the worst-case alignment and phantom placed above the Phone, hence exposed to Phone leakage.

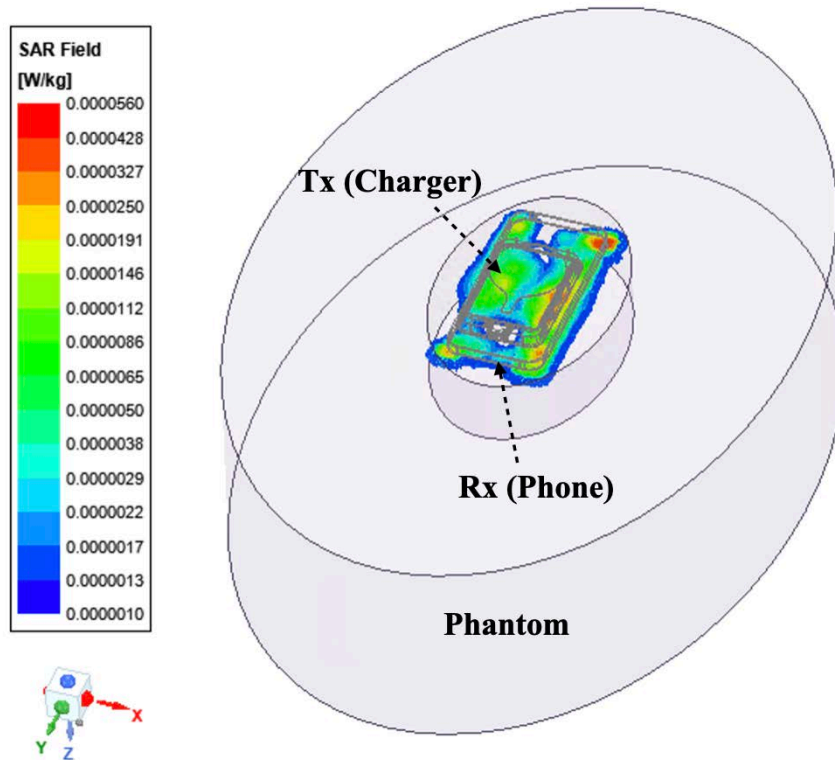
**Exposure Case 303 (b):** Misaligned configuration with the worst-case alignment and phantom placed below the Charger, hence exposed to Charger leakage.

Simulation results, SAR and E-field values for the four exposure cases are shown below.

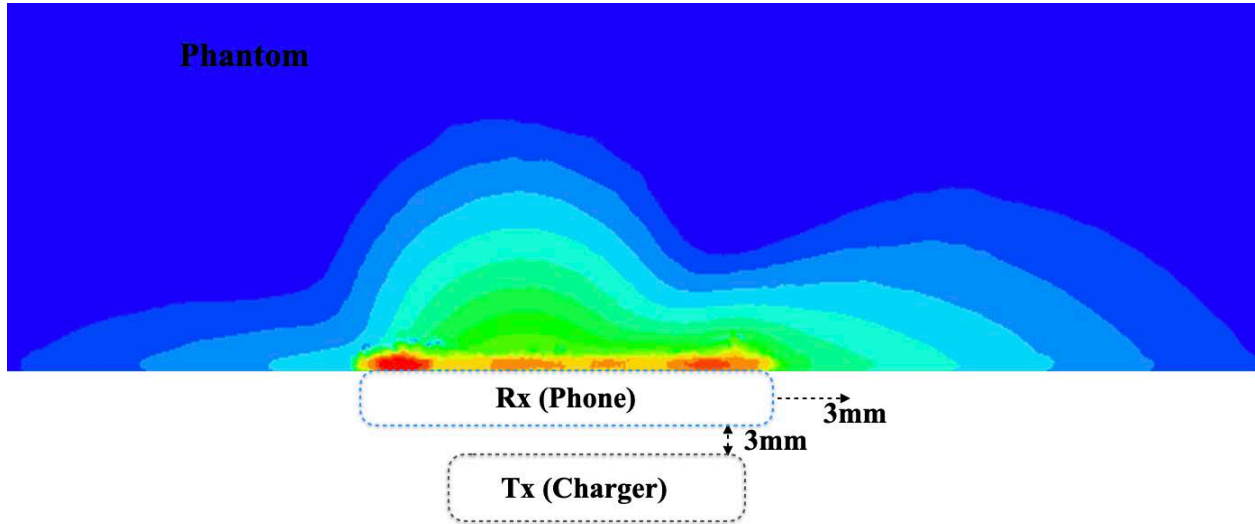
Table 6. Charger + Phone (5 W) at 360 kHz : Averaged 1-g SAR and E-field simulation results.

Exposure Case	Description	Peak Spatial Average SAR (W/kg) Averaged over 1 gram	Peak Spatial Avg E (V/m) Averaged over 2x2x2 mm <sup>3</sup>
Case 000 (a)		0.0000081	0.47
Case 000 (b)		0.0000001	0.025
Case 303 (a)		<b>0.000056</b>	0.8
Case 303 (b)		0.0000088	0.23

SAR plot (bottom view) is shown for Case303(a). The peak spatial 1-g average SAR is 0.000056 W/kg.



(a) Average SAR plot for Case 303 (a).



(b) Side view of average SAR plot for Case 303 (a).

Figure 11: Spatial 1-gram average SAR for Case 303 (a): (a) 3D view and (b) side view.

## 6.2 Charger connected to power adapter with Phone as Rx

Considering that the phantom can be in contact with the Phone or the back side of the Charger, there is a total of four scenarios.

**Exposure Case 000 (a):** Nominal configuration with perfect alignment and phantom placed above the Phone, hence exposed to Phone leakage.

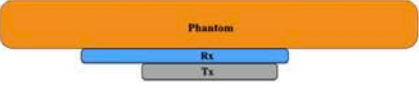
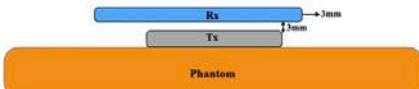
**Exposure Case 000(b):** Nominal configuration with perfect alignment and phantom placed below the Charger, hence exposed to Charger leakage.

**Exposure Case 303 (a):** Misaligned configuration with the worst-case alignment and phantom placed above the Phone, hence exposed to Phone leakage.

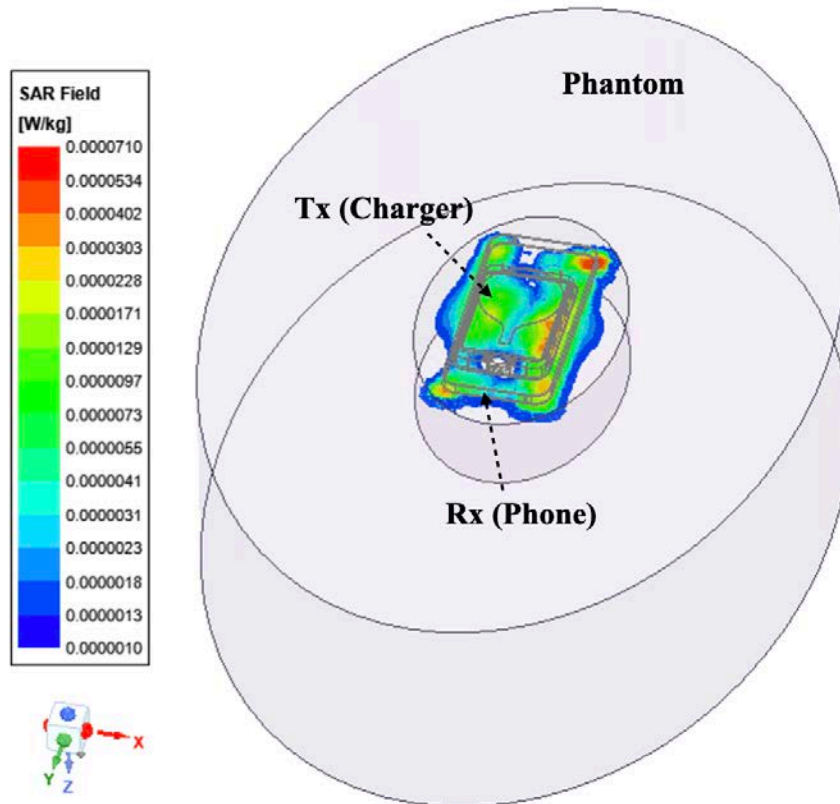
**Exposure Case 303 (b):** Misaligned configuration with the worst-case alignment and phantom placed below the Charger, hence exposed to Charger leakage.

Simulation results, SAR and E-field values for the four exposure cases are shown below.

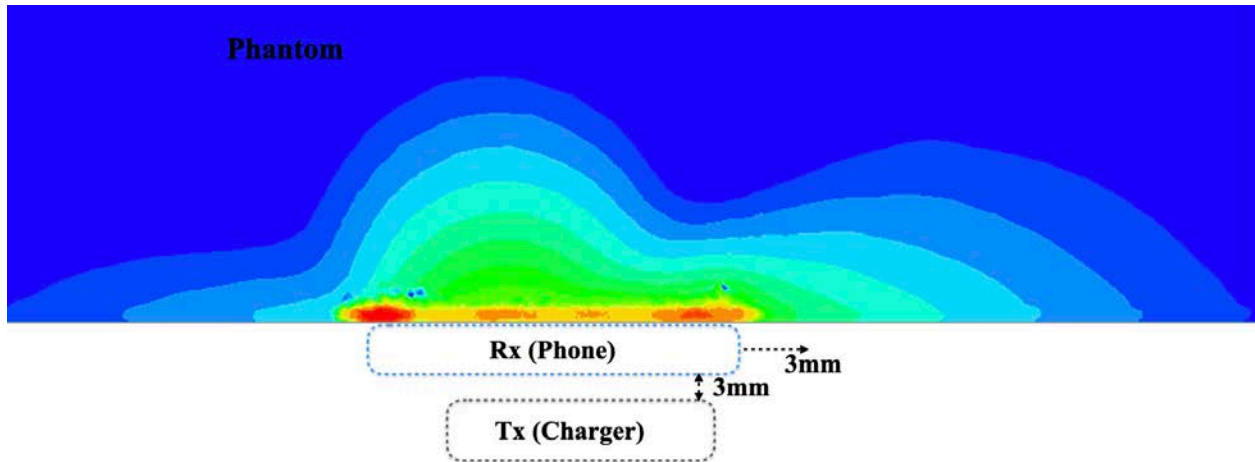
Table 7. Charger + Phone (15 W) at 360 kHz: Averaged 1-g SAR and E-field simulation results.

Exposure Case	Description	Peak Spatial Average SAR (W/kg) Averaged over 1 gram	Peak Spatial Avg E (V/m) Averaged over 2x2x2 mm <sup>3</sup>
Case 000 (a)		0.0000123	0.59
Case 000 (b)		0.00000016	0.031
Case 303 (a)		<b>0.000071</b>	0.84
Case 303 (b)		0.0000112	0.26

SAR plot (bottom view) is shown for Case303(a) below. The peak spatial 1-g average SAR is 0.000071 W/kg.



(a) Average SAR plot for Case 303 (a).



(b) Side view of average SAR plot for Case 303 (a).

Figure 12: Spatial 1-gram average SAR for Case 303 (a): (a) 3Ds view and (b) side view.

### 6.3 Additional Exposure Cases:

In addition, two corner cases were also investigated that are not likely to happen in normal application when the Charger is in direct contact with the phantom and the Charger is working with the highest current are investigated.

**Direct Exposure Case 1(a):** with receiver absent and the phantom placed directly above the Charger. The Charger is excited with the highest current level among all of the charging cases (i.e., 3 A)

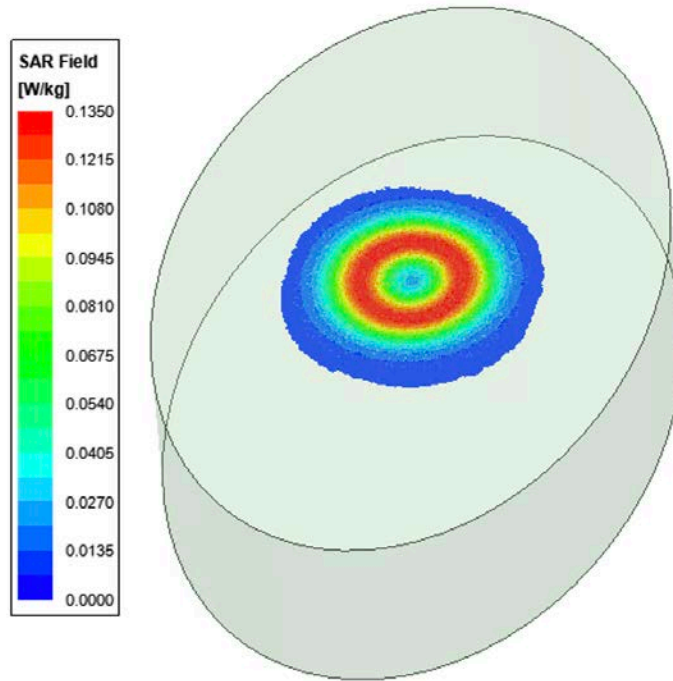
**Direct Exposure Case 1(b):** with receiver absent and the phantom placed below the Charger. The Charger is excited with the highest current level among all of the charging cases (i.e., 3 A)

Peak 1-g averaged SAR and E-field inside the Phantom for the Direct exposure cases are shown below.

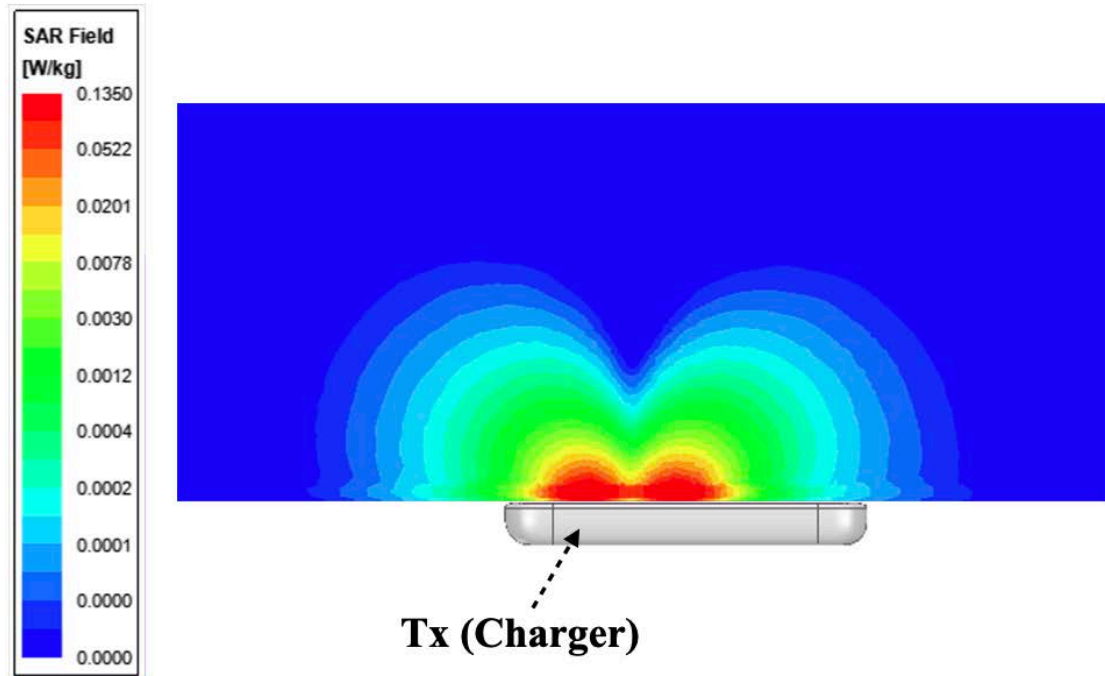
Table 8. Charger Only: Averaged 1-g SAR and E-field simulation results.

Exposure Case	Description	Peak Spatial Average SAR (W/kg) Averaged over 1 gram	Peak Spatial Avg E (V/m) Averaged over 2x2x2 mm <sup>3</sup>
Direct Exposure (unrealistic) Case 1(a)		0.135	37.8
Direct Exposure (unrealistic) Case 1(b)		0.00013	0.79

SAR plot for Direct Exposure Case 1(a) is shown below. The peak spatial 1-g average SAR is 0.1350 W/kg.



(a) Average SAR plot for Direct Exposure Case 1(a).



(b) Side view SAR plot for Direct Exposure Case 1(a).

Figure 13: SAR plot for Direct Exposure Case 1(a)

## 7 Summary

Based upon the above results, the accuracy of the SAR simulations is demonstrated by correlating H-field measurements to simulations. The validity of using this modeling and SAR computational method hence is established. For the nominal case where the Charger and the phone are aligned without any vertical separation, the highest peak spatial 1-gram average SAR is 0.0000123 W/Kg and the highest peak spatial average E field (i.e., averaged over a cube of 2 mm x 2 mm x 2 mm) is 0.59 V/m.

## 8 Annex A: Specific Information for SAR Computational Modelling

### 1) Computation Resources

The models were simulated on a 96 core CPU server with an available RAM of 4 Terabytes. Each model variation took around 12 hours to complete. Based on the simulation profile, the minimum resources needed to finish these simulations will be approximately 8 core CPU with 512 GB of RAM. Using the minimum requirements simulation will likely take more time than 12 hours.

### 2) Algorithm implementing and validation

This section is divided into two parts. The code performance validation provides methods to determine that the finite-element algorithm in HFSS has been implemented correctly and works accurately within the constraints due to the finite numerical accuracy. It further determines the quality of absorbing boundary conditions and certain parts of the post processing algorithms that are part of HFSS. The second part has few canonical benchmarks. All benchmarks can be compared to analytical solutions of the physical problem or its numerical representation. The methods characterize the implementation of the finite-element algorithm used by HFSS in a very general way. They are defined such that it is not possible to tune the implementation for a particular benchmark or application without improving the overall quality of the code.

#### 2.1) Code performance validation

##### 2.1.1) Propagation homogeneous medium

A straight rectangular waveguide with ports on both ends is well suited as a first test of an implementation of the Finite-Element Method used by HFSS. The waveguide has a width of 20 mm, a height of 10 mm and a length of 300 mm. The waveguide is filled homogeneously with a material which, in three separate simulations, shall assume the following properties:

- i.  $\epsilon_r = 1$ ,  $\sigma = 0$  S/m;
- ii.  $\epsilon_r = 2$ ,  $\sigma = 0$  S/m;
- iii.  $\text{Re}(\epsilon_r) = 2$ ,  $\sigma = 0.2$  S/m.

To verify that the mesh used by HFSS is independent of orientation, the waveguide has been rotated so that it is not parallel with any principal coordinate plane (XY, XZ, YZ). The waveguide is driven in the TE<sub>10</sub> mode at 10 GHz. Reported are the magnitudes of S<sub>21</sub> and S<sub>11</sub>, as well as the values of the real and imaginary parts of the propagation constant  $\gamma$ . The table 1, below provides the reference values [B1], acceptable result criteria, as well as the simulated results.

Table 9: Criteria for the waveguide evaluation

Re( $\epsilon_r$ )	1	2	2
$\sigma$	0	0	0.2
S21  reference value	1	1	$8.7 \times 10^{-5}$
Criterion for  S21	$\geq 0.9999$	$\geq 0.9999$	$\pm 5 \times 10^{-6}$
S21  simulated results	1	1	$8.7 \times 10^{-5}$
S11  reference value	0	0	0
Criterion for  S11	$\leq 0.003$	$\leq 0.003$	$\leq 0.003$
S11  simulated results	0	0	0
Re( $\gamma$ ) reference value	0	0	31.17 m-1
Criterion for Re( $\gamma$ )	$\pm 0.1$ m-1	$\pm 0.1$ m-1	$\pm 2\%$
Re( $\gamma$ ) simulated results	0	0	31.17
Im( $\gamma$ ) reference value	138.75 m-1	251.35 m-1	253.28 m-1
Criterion for Im( $\gamma$ )	$\pm 2\%$	$\pm 2\%$	$\pm 2\%$
Im( $\gamma$ ) simulated results	138.75	251.35	253.28

As is seen in the above table, HFSS easily meets the criteria for properly and accurately calculating the waveguide problem.

### 2.2.2) Planar dielectric boundary

In order to test the reflection of a plane wave by a dielectric boundary, a rectangular waveguide can again be used. It is well known that the TE<sub>10</sub> mode can be thought of as a superposition of two plane waves [1]. Each wave's direction of propagation makes an angle  $\theta$  with the axis of the wave guide, given by

$$\cos^2\theta = 1 - (c/2af)^2 \quad (1)$$

where  $c$  is the speed of light,  $a$  is the width of the wave guide and  $f$  is the frequency. Assuming the axis of the waveguide is the  $Z$  axis and assuming the waveguide is filled with vacuum for  $Z > 0$  and filled with dielectric 1 with complex relative permittivity  $\epsilon_r$  for  $Z < 0$ , Fresnel reflection coefficients for the TE and the TM cases, defined as ratios of electric field strengths, are given by [2]

$$R^{TE} = (k_{0,z} - k_{1,z}) / (k_{0,z} + k_{1,z}) \quad (2)$$

$$R^{TM} = (\epsilon_r k_{0,z} - k_{1,z}) / (\epsilon_r k_{0,z} + k_{1,z}) \quad (3)$$

where  $k_{0,z}$  and  $k_{1,z}$  denote the  $z$  component of the propagation vector of the plane wave in vacuum and in the dielectric, respectively. They can be evaluated through

$$k_{0,z} = k_0 \cos \theta \quad (4)$$

$$k_{1,z} = k_0 \sqrt{(\epsilon_r - \sin^2 \theta)} \quad (5)$$

Finally,  $\epsilon_r$  is complex and is given by

$$\epsilon_r = \text{Re}(\epsilon_r) - j\sigma / (2\pi f \epsilon_0) \quad (6)$$

where  $\text{Re}(\epsilon_r)$  denotes the real part of the relative permittivity and  $\sigma$  is the conductivity of the medium.

For this test, a 20 mm × 10 mm waveguide with a length of 60 mm, as shown in Figure 1, was created. The top half was filled with vacuum and the bottom half with dielectric.

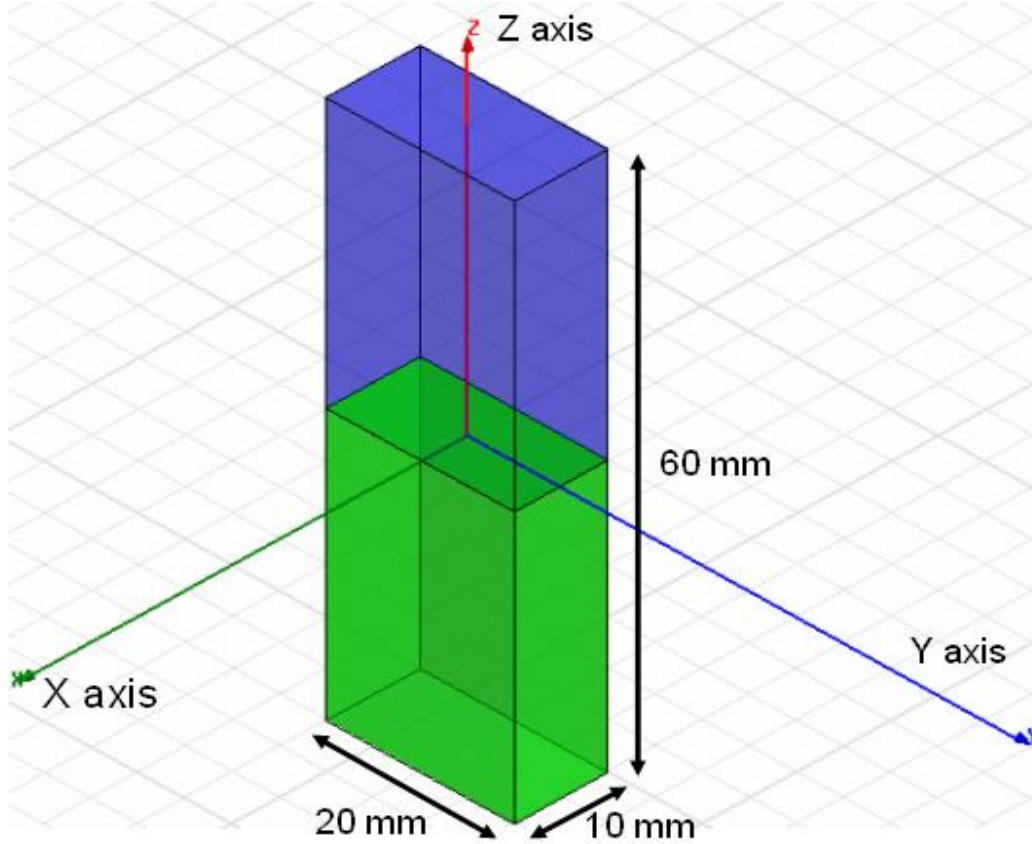


Figure 14: Waveguide filled half with vacuum and half with dielectric

In one copy of the model, all side walls were lossless metal, such that the dominant mode is the TE<sub>10</sub> mode with propagation constant 138.75 m<sup>-1</sup> at 10 GHz and represents the TE case in the reflection analysis. In the other copy of the model, the side walls that are parallel to the YZ plane were perfect magnetic conductors while the other walls were perfect electric conductors, such that the second mode (after a TEM mode which won't be used in this test) has propagation constant 138.75 m<sup>-1</sup> at 10 GHz and represents the TM case in the reflection analysis.

Before simulation, the waveguides were rotated over an arbitrary angle such that no face is parallel with any coordinate plane. The waveguides were driven at 10 GHz in the proper mode.

In doing so, it is good practice to calculate all propagating modes, but the coupling between modes is expected to be negligible. Simulations were run for the cases of lossless and lossy dielectric as shown in Table 2. For the HFSS to pass the test, according to IEC 62704-1, the results need to be within 2% of the analytical values given in Table 2.

Table 10: Reflection at a dielectric interface

Re( $\epsilon_r$ )	$\sigma$ (S/m)	RTE	RTE- Simulated	RTM	RTM - Simulated
4	0	0.4739	0.4739	0.1763	0.1763
4	0.2	0.4755	0.4755	0.1779	0.1779
4	1	0.5105	0.5105	0.2121	0.2121

As can be seen in table 2, HFSS produces results that are identical to the analytical results.

## 2.2) Canonical Benchmarks

The results for few low frequency benchmarks are summarized below. These benchmarks were used to validate the accuracy of the tool at low frequencies:

### 2.2.1) Dipole Antenna:

The following parameter were used in the dipole antenna to resonate at 400KHz.

Dipole length: 375 meters

Feed gap: 2.5 meters

Dipole Diameter: 5 meters

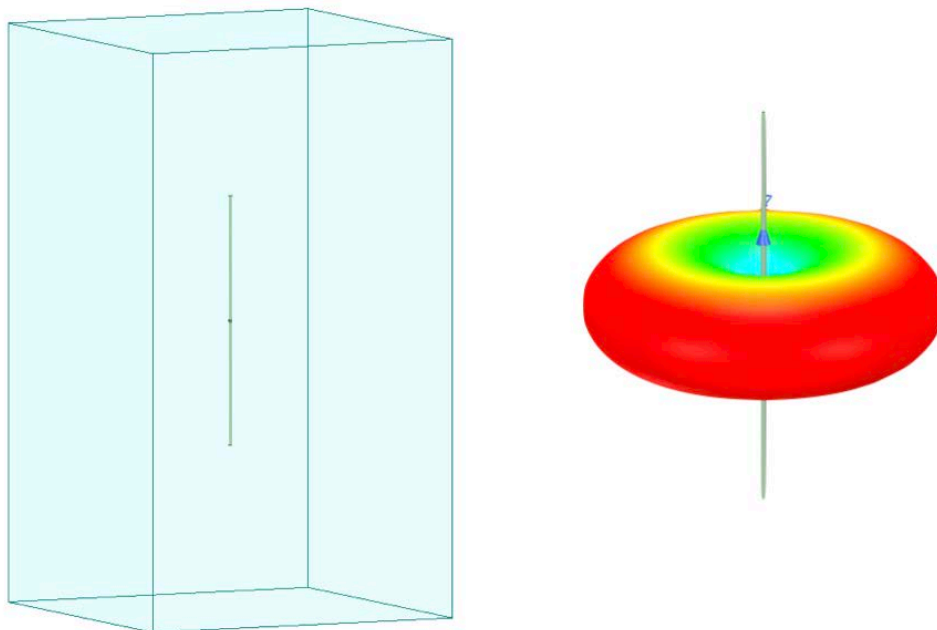


Figure 15: Dipole Antenna Model

The document IEC 62704-4 ED1 was referenced to compare the tables. Two computation methods were demonstrated as shown below to show the validity of the model.

Table 11: Simulated Dipole parameters

### FEM Solver

Quantity	Simulation results	Tolerance	Satisfied?
Re(Z) at 400 KHz	<b>94.09</b>		
Im(Z) at 400 KHz	<b>55.62</b>		
Re(Z) at 320 KHz	<b>39.26</b>	$25\Omega < Re(Z) < 50\Omega$	Yes
Im(Z) at 320 KHz	<b>-90.52</b>	$-50\Omega < Im(Z) < -100\Omega$	Yes
Re(Z) at 360 KHz	<b>59.58</b>	$50\Omega < Re(Z) < 75\Omega$	Yes
Im(Z) at 360 KHz	<b>-18.30</b>	$-25\Omega < Im(Z) < 0\Omega$	Yes
Frequency for Im(Z) =0	<b>370</b>	$360MHz < f < 380MHz$	Yes
Maximum power budget error	<b>0.3</b>	$< 5\%$	Yes

### MoM Solver

Quantity	Simulation results	Tolerance	Satisfied?
Re(Z) at 400 KHz	<b>98.45</b>		
Im(Z) at 400 KHz	<b>53.57</b>		
Re(Z) at 320 KHz	<b>43.31</b>	$25\Omega < Re(Z) < 50\Omega$	Yes
Im(Z) at 320 KHz	<b>-90.55</b>	$-50\Omega < Im(Z) < -100\Omega$	Yes
Re(Z) at 360 KHz	<b>65.03</b>	$50\Omega < Re(Z) < 75\Omega$	Yes
Im(Z) at 360 KHz	<b>-18.59</b>	$-25\Omega < Im(Z) < 0\Omega$	Yes
Frequency for Im(Z) =0	<b>370</b>	$360MHz < f < 380MHz$	Yes
Maximum power budget error	<b>0.02</b>	$< 5\%$	Yes

### 2.2.2) Toroid Inductor:

The parameters of the toroid were chosen to be

$$N = 20$$

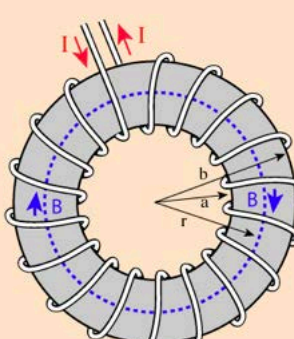
$$A = 6.35e-4 \text{ m}^2$$

$$R = 0.0263 \text{ m}$$

$$\mu_r = 64$$

The formula below gave an inductance of 139uH. The model created in HFSS gave an inductance of 139.9uH.

**Approximate Inductance of a Toroid**



Finding the [magnetic field](#) inside a [toroid](#) is a good example of the power of [Ampere's law](#). The current enclosed by the dashed line is just the number of loops times the current in each loop. Ampere's law then gives the magnetic field at the centerline of the toroid as

$$B2\pi r = \mu NI$$

$$B = \frac{\mu NI}{2\pi r}$$

The [inductance](#) can be calculated in a manner similar to that for any [coil of wire](#).

The application of [Faraday's law](#) to calculate the voltage induced in the toroid is of the form

$$Emf = -N \frac{\Delta\Phi}{\Delta t} = -NA \frac{\Delta B}{\Delta t}$$

This can be used with the magnetic field expression above to obtain an expression for the inductance.

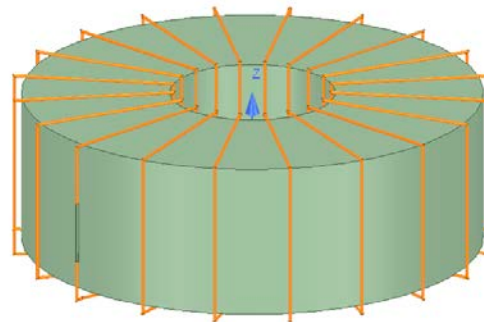
$$L \approx \frac{\mu N^2 A}{2\pi r} \quad \begin{array}{l} A = \text{cross-sectional area} \\ r = \text{toroid radius to centerline} \end{array}$$


Figure 16: Toroid Model

### **2.2.3) Circular coil parallel to a flat, homogeneous phantom:**

The following benchmark is implemented using Equations 1-4 of the referenced Chen et al. (2014) paper and also matches Figure 6 therein scaled to 10 coil turns.

Below is the coil and phantom parameters:

Coil Diameter: 50 mm  
Number of Turns: 10  
RMS Current: 0.707 A (Peak current = 1 A)  
Frequency: 100 kHz  
Coil-to-Body Distance: 5 mm  
Tissue Conductivity: 0.05 S/m  
Tissue Permittivity: 1120

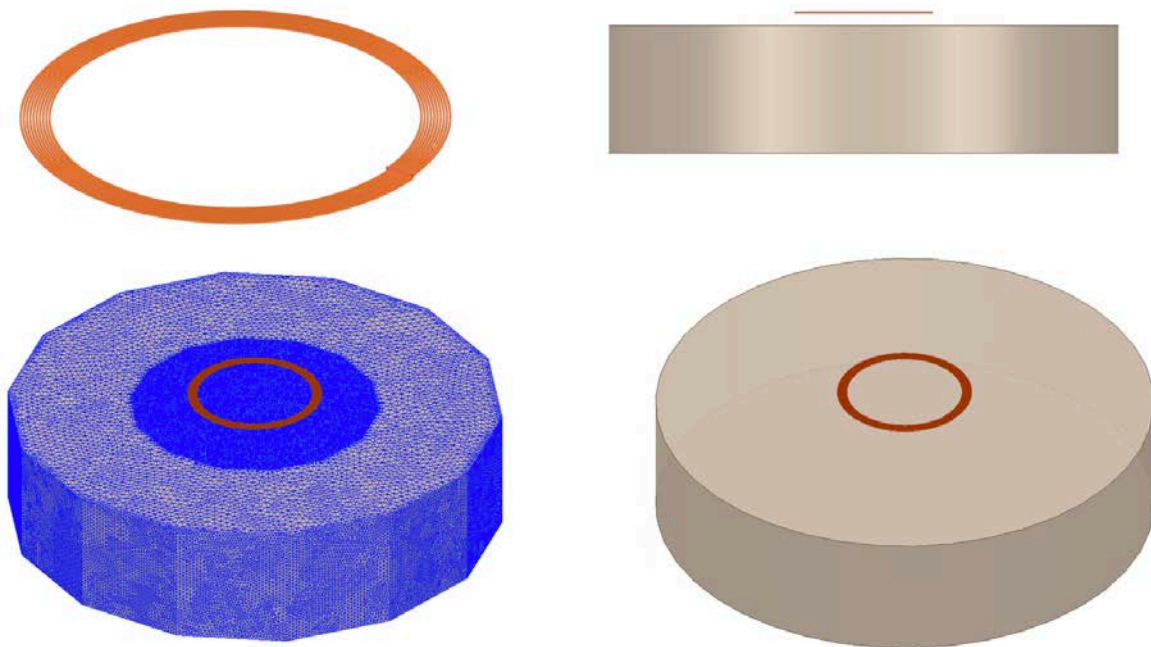


Figure 17: Current loop in front of a cuboid

The simulated spatial peak RMS electric field in tissue is 1.51 V/m compared to the analytical 1.47 V/m.

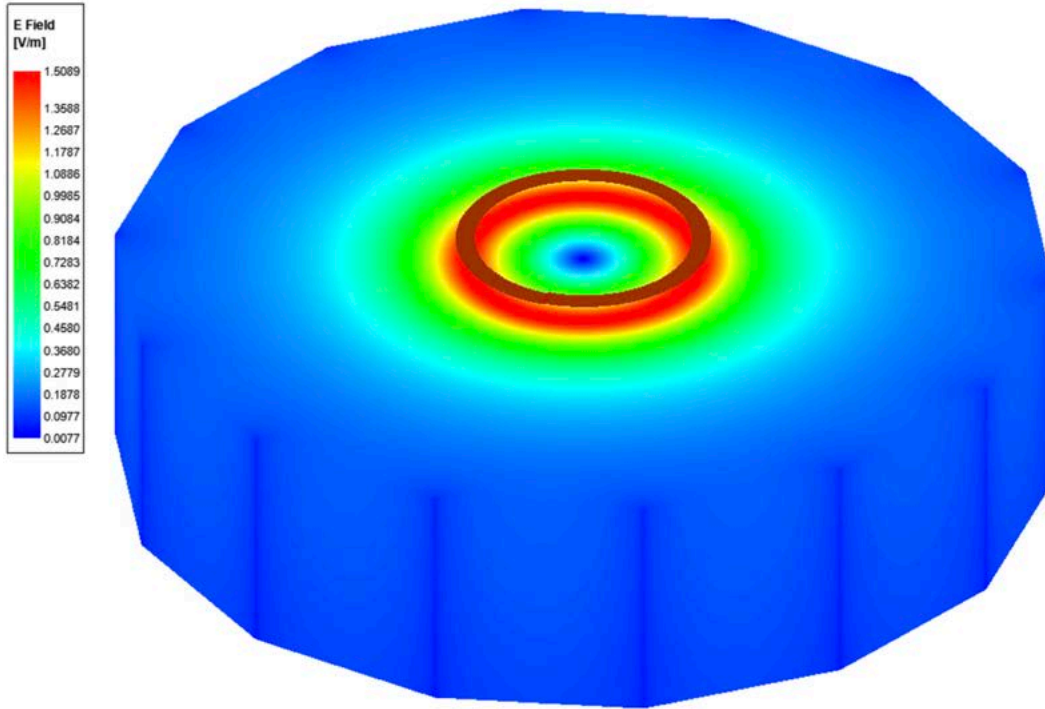


Figure 18: Current Density plot

### 3) Computational peak SAR from peak components & One-gram averaged SAR procedure

The calculation method for SAR follows IEEE P1528.4. Once the solver calculated the S-Parameter results, different coils can be driven and the result from the S-Parameter calculation is automatically scaled to the driving current of the coils. This result combination provides the correctly scaled power loss density in the phantom. The SAR calculation computes the local SAR first using electric field and conducting current:

$$SAR = \vec{E} \bullet \vec{J}_{con,j} / (2\rho)$$

Afterwards the local SAR is averaged over a specific mass, usually 1g or 10g. As described in [IEEE P1528.4] the mass averaging is done by mapping the results to a structured hexahedral grid and afterwards the averaging scheme for FDTD per [IEEE P1528.4] is applied. The SAR calculation on the hexahedral grid is compliant with IEC 62704-1.

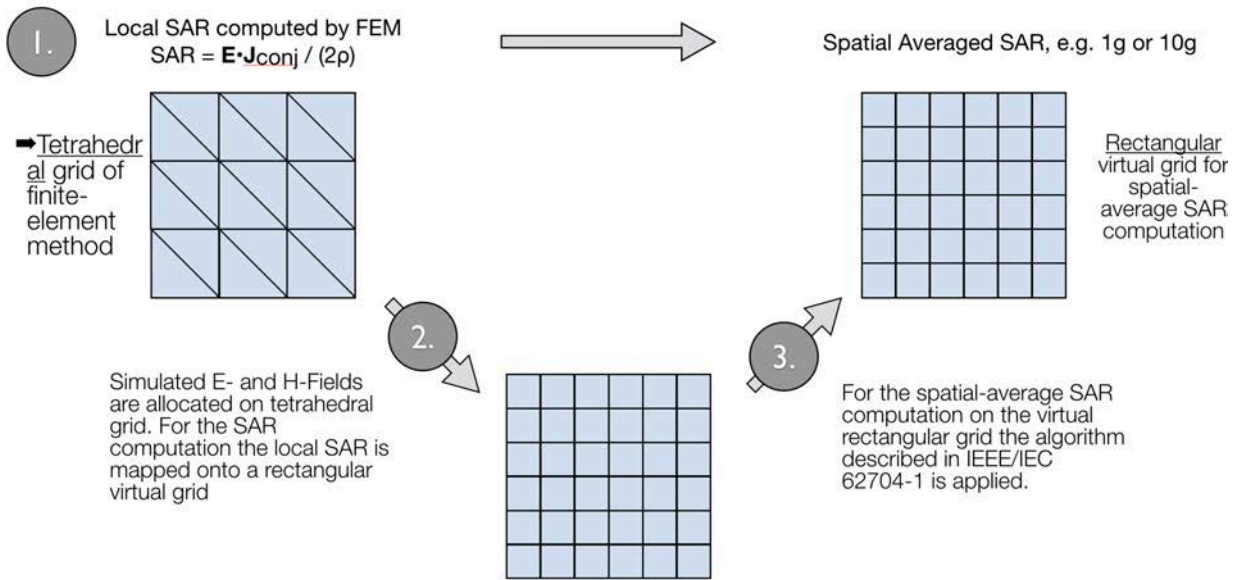


Figure 19: IEEE P1528.4 for SAR computation

#### 4) Total Computational Uncertainty

Below is a table summarizing the budget of the uncertainty contributions of the numerical algorithm and of the rendering of the simulation setup. The table was filled using the IEC 62704-4 ED1 from 2018.

For the simulations, the direct exposure case where the phantom is placed directly in front of the puck is considered.

Table 6. Budget of uncertainty contributions of the numerical algorithm (filled based on IEC 62704-4 ED1).

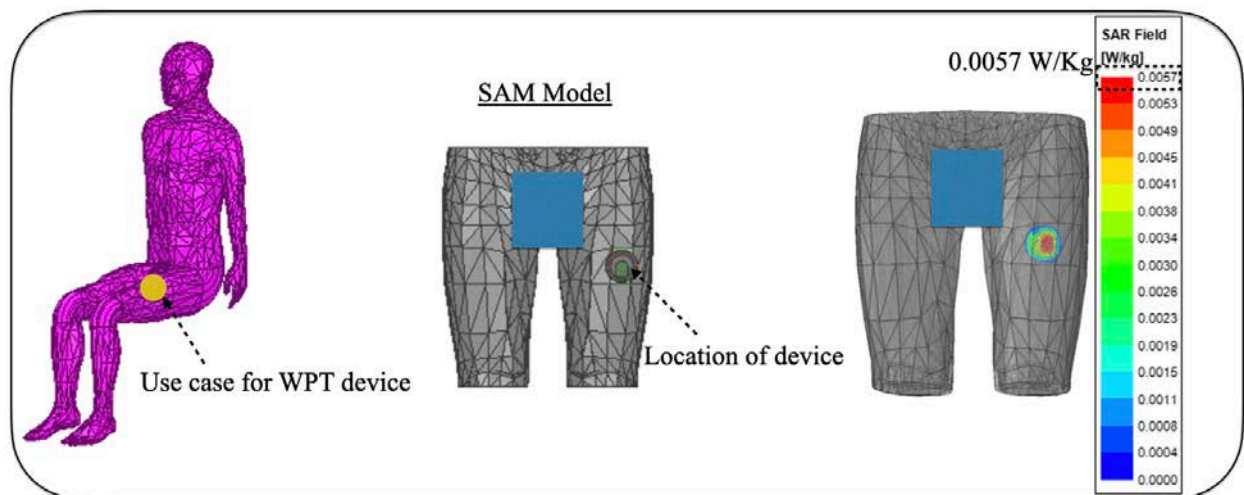
a	b	d	e	g
Uncertainty component	Subclause	Probability distribution	Divisor f(d, h)	Uncertainty %
Mesh resolution	7.2.3	N	1	<b>0.01</b>
ABC	7.2.4	N	1	<b>0.08</b>
Power budget	7.2.5	N	1	<b>0.0</b>
Convergence	7.2.6	R	1,73	<b>0.01</b>
Phantom dielectrics	7.2.7	R	1,73	<b>0</b>
Combined standard uncertainty ( $k = 1$ )				<b>0.1</b>

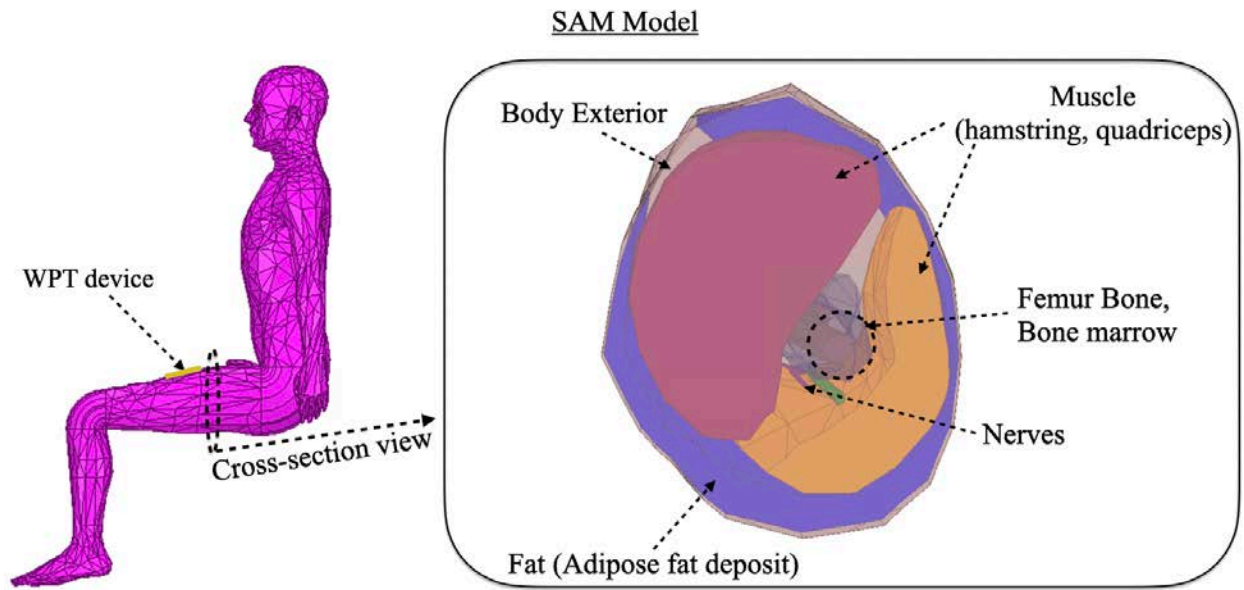
Below is a table summarizing the budget of the uncertainty of the developed model. The table was filled using the IEC 62704-4 ED1 from 2018.

Table 7. Measurement uncertainty table.

<b>a</b>	<b>b</b>	<b>d</b>	<b>e</b>	<b>g</b>
<b>Uncertainty component</b>	<b>Subclause</b>	<b>Probability distribution</b>	<b>Divisor f(d, h)</b>	<b>Uncertainty %</b>
Uncertainty of the DUT model (based on near field distribution)	7.2.2	N	1	<b>2.12</b>
Uncertainty of the measurement equipment and procedure	7.2.3	N	1	<b>4</b>
Combined standard uncertainty ( $k = 1$ )				<b>6.12</b>

SAR calculations are also performed using specific standard anthropomorphic model (SAM) for the use-case of the WPT device described in this report. The use-case for the WPT device is shown in below. SAM accurate model with appropriate frequency-dependent SAM tissue dielectric properties are used in the simulation [Ref. 3]. The average SAR is calculated for the worst-case scenario with peak current of 3A as the input excitation source for the coil. The average SAR value is 0.0057 W/Kg. The SAR values from anatomical model is much lower than worst case scenario used in the main section, which only impacts the uncertainty calculation in the negative direction, making the presented data in section 6 always representing worst case numbers.





References:

- 1) The electrical conductivity of human cerebrospinal fluid at body temperature, S.B. Baumann; D.R. Wozny; S.K. Kelly; F.M. Meno, IEEE Transactions on Biomedical Engineering ( Volume: 44 , Issue: 3 , March 1997 )
- 2) C.Gabriel, S.Gabriel and E.Corthout: The dielectric properties of biological tissues: I. Literature survey, *Phys. Med. Biol.* 41 (1996), 2231-2249.
- 3) S.Gabriel, R.W.Lau and C.Gabriel: The dielectric properties of biological tissues: II. Measurements in the frequency range 10 Hz to 20 GHz, *Phys. Med. Biol.* 41 (1996), 2251-2269.
- 4) S.Gabriel, R.W.Lau and C.Gabriel: The dielectric properties of biological tissues: III. Parametric models for the dielectric spectrum of tissues, *Phys. Med. Biol.* 41 (1996), 2271-2293.
- 5) <https://itis.swiss/virtual-population/tissue-properties/database/thermal-conductivity/>
- 6) <http://hyperphysics.phy-astr.gsu.edu/hbase/magnetic/toroid.html>
- 7) X. L. Chen et al., "Human Exposure to Close-Range Resonant Wireless Power Transfer Systems as a Function of Design Parameters," in *IEEE Transactions on Electromagnetic Compatibility*, vol. 56, no. 5, pp. 1027-1034, Oct. 2014.